

Additive Manufacturing of Ti-6Al-4V Using a Pulsed Laser Beam

ABDALLA R. NASSAR and EDWARD W. REUTZEL

Microstructural development in directed-energy additive manufacturing of metal components is a complex process that produces parts with materials whose microstructure and properties are influenced by multiple heating and cooling cycles. Much work has been undertaken to correlate microstructural development with processing conditions, such as laser power and processing speed. Here, the microstructure and indentation hardness of a Ti-6Al-4V component processed with a pulsing laser beam and a continuous wave (CW) laser beam are investigated. It is found that the pulsed-beam build showed no statistically significant variation in lath width or indentation hardness with build height while the build deposited with the CW beam showed a statistically significant decrease in hardness and an increase in lath width near the middle of the build. The reduction in variability with beam pulsing is attributed to rapid cooling rates within the melt pool, a greater degree of melt pool stirring, and reduced aging during part build-up.

DOI: 10.1007/s11661-015-2838-z

© The Minerals, Metals & Materials Society and ASM International 2015

I. INTRODUCTION

ADDITIVE manufacturing (AM) of metal components has gained much attention in recent years, with metal-based AM machine sales increasing by 75 pct from 2012 to 2013.^[1] This can, in part, be attributed to the ability to rapidly produce high-value components directly from a digital CAD model. Metal components are commonly built using one of two methods: powder-bed fusion or directed-energy deposition.^[2] In the former, a laser or electron beam is scanned over a bed of powder; while in the latter, powder is blown or wire is fed into the melt pool formed by a laser or electron beam. In both cases, parts are built up layer-by-layer.

Though processing itself is straight-forward, the resulting internal part microstructure can be complex and non-uniform. Parts produced using AM undergo multiple, complex thermal cycles which can result in internal variations in microstructure and properties. Such intra-build variations have been observed to depend on part orientation, part size, and the scanning pattern used for part build-up. Intra-build variations have been witnessed in both powder-bed and directed-energy processes.

Of particular interest is the study of intra-build variations in AM-produced titanium alloy titanium-6 pct aluminum-4 pct vanadium (Ti-6Al-4V) components. This alloy, also known as Grade 5 titanium, is favored in biomedical, aerospace, and defense application, due to its non-toxicity, low weight, high strength-to-density ratio, and low creep at high temperatures.

Within Ti-6Al-4V, microstructural variation is characterized by the size, shape, orientation, and ratio of the α - and β -phases, prior-beta grain structure, as well as the existence of the diffusionlessly transformed α' phase. Details of microstructural features can be correlated to the mechanical properties of Ti-6Al-4V.^[3] Typically, the microstructure of additively manufactured Ti-6Al-4V components consists of Widmanstätten α - β , with β present between narrow α -laths, and large, columnar, prior-beta grains extending from the bottom to the top of builds.^[4]

A. Intra-build Variations in AM of Ti-6Al-4V

Intra-build variations, such as a transition from a Widmanstätten to a martensitic α' microstructure, have been observed to occur near the top surface of parts produced using the Arcam, powder-bed, electron-beam-melting (EBM) process.^[4] Also using EBM, Murr *et al.*^[5] reported a 1.5 to 2 times increase in α -lath width from the bottom to the top of a 6.8-cm tall, cylindrical build—measurements were made 1 cm from the bottom and 1 cm from the top of the build. Alpha-lath widths have also been reported to vary from interior to exterior build locations along the same build height.^[6]

Variations in microstructure have also been observed in the directed-energy, laser engineered net shaping (LENS[®]) process. Qian *et al.* reported that the α -lath width was larger in the middle than at the bottom or top of single-wall builds.^[7] Using a powder-blown, directed-energy deposition (DED) process, similar to LENS but with much higher power (11 kW rather than ~500 W in the case of Reference 7), Kelly and Kemp^[8] also observed smaller α -laths near the top of a single-wall build and a grading of α -lath widths within each deposited layer. They argued that layer bands (dark, periodic lines perpendicular to the build direction) were due to a change in morphology from a Widmanstätten α to a colony α morphology, caused by a slow cooling rate from above the β transus temperature. They further

ABDALLA R. NASSAR, Research Associate, and EDWARD W. REUTZEL, Head of Laser System Engineering & Integration Department, are with the Applied Research Laboratory, The Pennsylvania State University, University Park, PA 16804. Contact e-mail: arn5000@psu.edu

Manuscript submitted October 9, 2014.

Article published online March 13, 2015

argue, and present a numerical model^[9] as further evidence that this banding occurs, not during the deposition of the layer on which it is observed, but as a result of reheating of buried layers during deposition of subsequent layers above the α dissolution temperature—the temperature in the α - β region where α begins transforming into β —but below the β transus temperature. For this reason, henceforth, these banded features are referred to as reheating bands.

Intra-build variations in the microstructure can be expected to correspond to variations in mechanical properties. Variations in indentation hardness and microstructure within AM builds have been shown across a range of AM processes, ranging from high-deposition-rate, multi-kilowatt-electron-beam-based processes to low-deposition-rate, powder-bed processes.^[10] For example, Murr, *et al.*^[5] reported that Vickers hardness decreased from the bottom to the top of Ti-6Al-4V builds produced using the ARCAM electron beam melting (EBM) process. Depending on processing conditions, hardness varied from the bottom to the top of build by 0.4 to 1 GPa (30 to 100 HV).^[5] Using the same process, Hrabec and Quinn^[6] reported a decrease in hardness, from exterior to interior build locations along the same build height, along with a counterintuitive decrease in α -lath thickness.^[6] Conversely, using the LENS process to build a single-wall in H13 tool steel, a decrease in hardness from the top surface of the build to the substrate has been reported.^[11,12] Variations in mechanical properties, such as strength and ductility, have also been shown to be influenced by part shape and size.^[13]

B. Influence of Beam Modulation

A comprehensive model linking processing conditions with resulting microstructure and mechanical properties has not yet been developed. However, it is well known that microstructure formation is governed by material temperature, time, thermal gradients, cooling rate, induced stresses, and melt pool dynamics. Given this, variations in beam power can be expected to influence microstructure. Results from investigations of laser, electron beam, and arc-welding support this assertion. Peak power density during laser welding of Ti-6Al-4V has been shown to influence microstructure and hardness.^[14] Arc modulation, arc pulsing,^[15] and magnetic stirring^[16] have also been reported to enhance flow within the melt pools and result in refined grain structures. It is thought that refining may occur through dendrite fragmentation, multiple cycling through the α - β transus, reduced weld-pool thermal gradients, or changes in the direction of the maximum thermal gradient.^[17] Sundaresan *et al.*^[15] argue that reduced and changing direction of the thermal gradient, through melt pool stirring, are more likely to contribute to grain refinement.

Recently, Mitzner *et al.*^[18] investigated beam and arc modulation in electron beam and gas tungsten arc additive manufacturing, respectively. They found that α -lath width was reduced with current modulation; prior-beta grain boundaries became more equiaxed; and, hardness values, as measured in the Y - Z , X - Z , and X - Y planes (where $+Z$ is the build-up direction) became

more isotropic with modulation. It should be noted that hardness values were averaged across a cross section in the “steady-state region” taken in each plane. The “steady-state region” was presumably the region near the center of the build.

Here, we investigate the use of laser-beam pulsing as a means to refine part microstructure and to reduce intra-build variations in Ti-6Al-4V builds deposited using a powder-blown DED process. This is done through comparison of two builds, each processed with identical energy input per unit length (average power/speed), but different laser-modulation modes. One build was processed using a continuous wave (CW) beam while the other was processed using a pulsed beam. The macrostructure (Section III-A), microstructure (Section III-B), and indentation hardness profiles (Section III-C) of each are compared and contrasted to understand the effects of laser-beam pulsing.

II. EXPERIMENTAL METHODOLOGY

A. Physical Setup

An Optomec LENS MR-7, laser-based, directed-energy-deposition system was used for deposition. The system was equipped with a 500-watt Ytterbium-doped fiber laser (IPG YLR-500-SM) which was focused to a second-moment spot diameter of 0.62 mm at a distance of 20.7 mm above the substrate. Beam size measurements were made using a PRIMES GmbH FocusMonitor. As shown in Figure 1, the laser spot size was 1.24 mm at the working distance, which corresponded to a space of 9.27 mm between the substrate and four, radially symmetric powder-delivery nozzles. Nozzles had an exit orifice diameter of 1.2 mm and were oriented at 18.25 deg with respect to the laser-beam propagation direction. Centered among the powder nozzles was a 6.35 mm diameter, center-purge nozzle, through which 30 lpm of argon flowed.

During deposition, the substrate was in the X - Y plane while the laser processing head remained stationary. After each layer deposition, the laser head was translated upward (in the $+Z$ -direction) by a predefined layer increment.

B. Materials

Ti-6Al-4V structures were deposited atop Ti-6Al-4V substrates. Annealed and ground-finished, 3.175 mm thick, substrates were used. Prior to processing, substrates were cleaned with acetone and isopropyl alcohol. Extra low interstitials (ELI)-grade powder was obtained from Phelly, Inc. Mean powder particle size was measured, using a Horiba LA950 particle size distribution analyzer, at 126.8 μm with a standard deviation of 45.94 μm .

C. Process Parameters

The processing chamber held an argon atmosphere, with an oxygen concentration below 20 parts per million, and a gauge pressure between 498 and 748 Pa

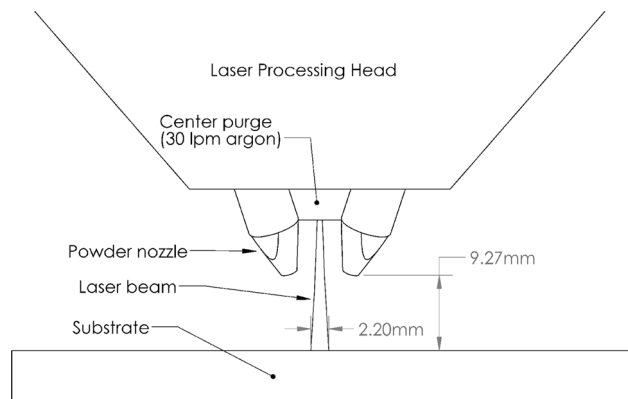


Fig. 1—Physical setup of processing head and laser beam with respect to the substrate.

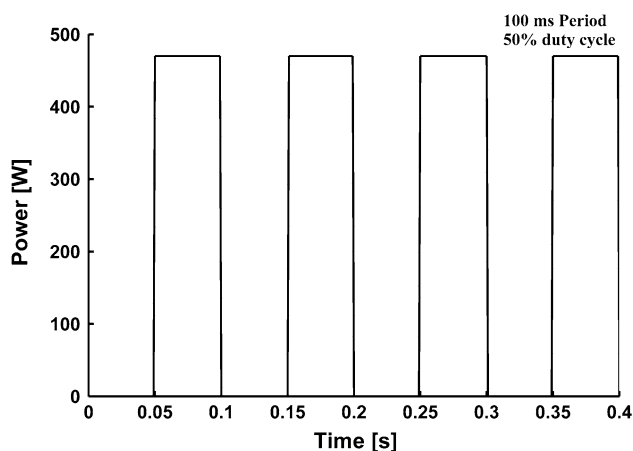


Fig. 2—Laser power in pulsed mode.

(2 to 3 in. of water). The pressure was maintained using a pressure regulator along with inlet flows of argon from the coaxial purge nozzle and the powder-delivery nozzles. Powder flow was measured and maintained at 3 g per minute using a powder feeder assisted by a 4-lpm argon flow.

Builds were deposited in one of two configurations. In the first, the laser was operated in CW mode, at a measured output power of 450 ± 25 W, and a processing speed of 10.58 mm/s (25 in./min). In the second, the laser power was modulated to produce periodic, square waves with a period of 100 ms and a duty cycle of 50 pct. Power as a function of time is plotted in Figure 2. To maintain the same energy input per unit traverse length as in CW mode, the processing speed was reduced to 5.29 mm/s (12.5 in./min) in pulsed mode.

D. Part Geometry and Build Plan

A rectangular block, 34.29 mm in length and 12.5 mm in width, with an internally varying hatch spacing was selected for deposition. The block was built-up using a total of 35 layers with layer increment

set point of 0.178 mm. It may be noted that the actual build height of each block exceeded the product of the layer increment by the number of layers. This layer increment was intentional set slightly below the anticipated layer thickness to account for, and take advantage of, the self-regulating nature of powder-blown DED.

On each layer, a total of twenty-six parallel hatches were deposited using a back-and-forth raster. The hatch order was reversed from layer to layer. Each hatch was 12.5 mm long, extending along the width of the block. This geometry was selected as part of unrelated work on defect detection, which will not be discussed in this article. For the present study, only the first set of six hatches, spaced center-to-center 0.914 mm apart, are of interest.

E. Characterization

Builds were cross-sectioned midway through the width of the part and perpendicular to the hatches. Cross sections were ground and polished according to standard metallographic techniques and drop etched using Krolls reagent. Microstructure was characterized using an optical microscope equipped with a digital camera. Micrographs were captured at each reported build height. Image contrast was enhanced using contrast stretching, and, to correct for non-uniform illumination, contrast-limited adaptive histogram equalization (CLAHE) was applied, as necessary, within the MATLAB (R2014a) software package. Reported alpha-lath widths were manually measured at 35 random locations within each image. Hardness indents were made at each reported build height, near where micrographs were recorded. Vickers hardness was measured using a LECO-M-400-G1 hardness tester using a load of 1 kgf applied for 10 seconds. Each reported hardness value is based on the average of five measurements along each reported build height.

III. RESULTS

A. Macrostructure

Polished and etched cross sections of the as-deposited builds are shown in Figure 3. The height of the CW build (Figure 3(a)) peaked around the third hatch at a height of 9.93 mm whereas the height of the pulsed-beam build (Figure 3(b)) peaked around the second hatch at a height of 9.65 mm.

Cross sections of both builds were characterized by columnar prior- β grain boundaries. The prior- β grains were on the order of a millimeter in width and extended several millimeters from the bottom of the build (above the heat-affected zone (HAZ)) to the top of the deposit. Approximately, seven prior-beta grains were present across the first six hatches of the CW build while eight prior-beta grains spanned across the six hatches of the pulsed-beam build.

Within and across the prior-beta grains, reheating bands were distinguished as dark regions extending

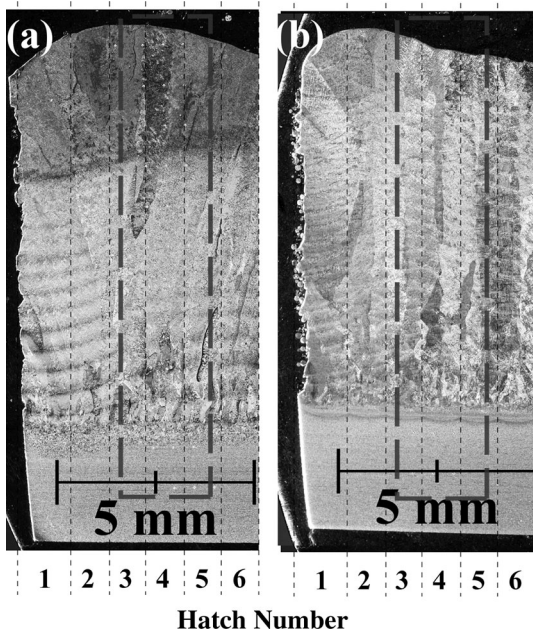


Fig. 3—Macrostructure of build deposited using (a) CW laser and (b) pulsed laser beam. Gray, dashed boxes indicate locations of hardness indents.

horizontally though the cross sections. In the case of CW build, layer bands were not observed 2.5 to 3.5 mm from the top surface of the build. In the case of the pulsed-beam build, reheating bands extended nearly to its top surface.

B. Microstructure

The microstructure of both the CW and pulsed-beam builds were characterized by thin α -laths oriented in a Widmanstätten basket-weave pattern. High-magnification micrographs are shown at several build heights for the CW build in Figure 4 and for the pulsed-beam build in Figure 5.

The primary distinction between the builds is the size of α -laths. Alpha-laths in CW build (Figure 4) were wider than in the pulsed-beam build (Figure 5). In the CW build, α -laths also varied in size with build height, appearing widest near the middle of the build (Figure 4(c)) and narrowest near the top (Figure 4(f)). In contrast to this, α -laths in the pulsed-beam build appeared similar irrespective of build height.

Measurements of the α -lath widths, using the micrographs in Figures 4 and 5, confirmed that α -lath widths varied significantly with build height in the CW build but not in the pulsed-beam build. The widths of α -laths as a function of distance from the top surface, for both builds, are shown as box plots in Figure 6. Near the top of the CW build, 1.5 mm from the top surface, the α -lath width was $0.78 \mu\text{m}$. It then peaked at a distance of 5.5 mm from the top surface, reaching $1.54 \mu\text{m}$, before falling to $1.27 \mu\text{m}$ at 9.5 mm from the top surface, near the substrate. In the pulsed-beam build, the α -lath width

averaged near $0.62 \mu\text{m}$ at all locations (within $+0.08/-0.04 \mu\text{m}$).

An analysis of variance (ANOVA), assuming a 95 pct confidence interval, showed that in the CW deposit there was a statistically significant variation of lath width with build height. The ANOVA p value was 1.12×10^{-20} . In contrast to this, the pulsed-beam build showed no significant variation in lath width with build height (p value of 0.142).

Possible differences in α -lath widths within and between reheating bands were also tested for statistical significance. Figure 7 juxtaposes micrographs taken at reheating band locations with those taken outside the banded region at a nearby location. The micrographs were taken approximately 6.5 mm from the top surface of the CW build and 4.5 mm from the top surface of the pulsed-beam build. Diffuse illumination was used in Figure 7, α appears black while inter-granular β appears white.

In both the CW and pulsed-beam builds, statistically significant differences were found in mean α -lath width within compared to between reheating bands. In the CW build, within the banded region the α -lath width averaged $1.0 \mu\text{m}$ (stdev = 0.22). Between the banded region, the lath width was larger, averaging $1.22 \mu\text{m}$ (stdev = $0.30 \mu\text{m}$). Although differences were within one standard deviation, an unpaired t test p value of 0.0014 established that the difference was statistically significant. Within the pulsed-beam build, α -lath width averaged $0.52 \mu\text{m}$ (Stdev = $0.10 \mu\text{m}$) within the banded region and $0.61 \mu\text{m}$ (Stdev = $0.16 \mu\text{m}$) between the banded region. As in the CW build, the difference in mean values was within one standard deviation but statistically significant (unpaired t test p value = 0.0056).

Qualitatively, it also appeared that regions within the darker, reheating bands contained more aligned α -platelets, known as colony alpha, than regions outside the bands—quantitative measurement was not attempted. If true, this is in agreement with the observations of Kelly and Kemp.^[8] The higher percentage of colony α within reheating bands may be responsible for their darker appearance under diffuse lighting. That is, light is preferentially scattered along specific directions from aligned plates, resulting in a darker appearance when the direction of scattering was not toward the observer. Between reheating bands, the orientation of alpha platelets may be more random resulting in light being scattered more uniformly.

C. Indentation Hardness

Vickers hardness was measured starting at 0.5 mm for the top of each build to the substrate, at 1 mm increments. At each height increment, five hardness measurements were recorded. Results are shown as box plots in Figure 8. An ANOVA analysis of hardness showed that, from 0.5 to 8.5 mm below the surface of the CW build, there was a statically significant variations in hardness with distance ($p = 0.0057$). In the CW build, hardness was highest near the top surface; at 0.5

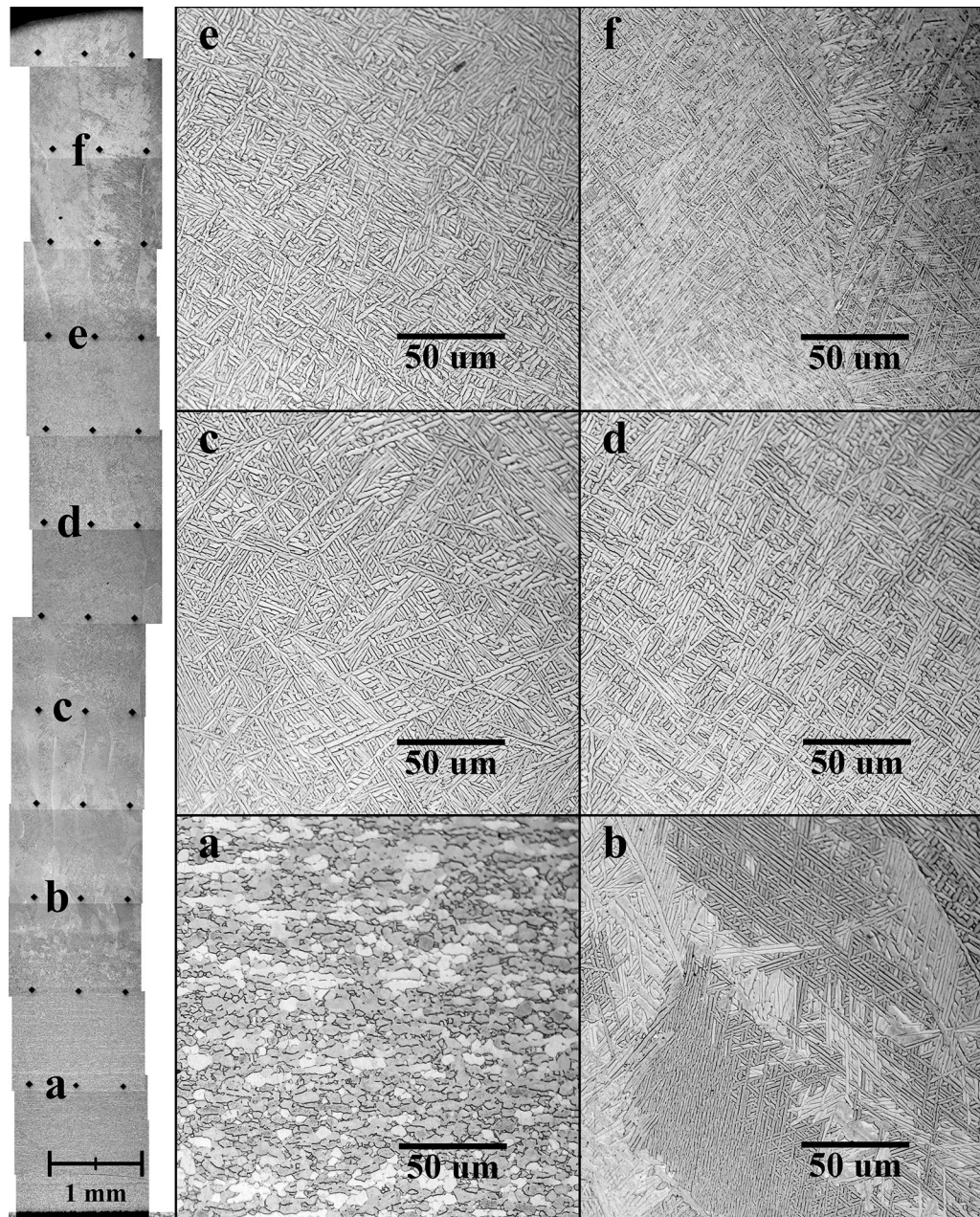


Fig. 4—Micrographs of the build processed using a CW laser beam. High-magnification images are shown for the locations indicated on the left-hand-side of the figure.

and 2.5 mm from the top surface, hardness peaked at 319 and 321 HV, respectively. Hardness was lowest in the middle of the build; at 5.5 mm from the top surface hardness dropped to 299 HV. Hardness increased from the middle of the build to the substrate until reaching the substrate hardness of 326 HV.

For the pulsed-beam build, there were no significant changes in hardness values with distance ($p = 0.37$) from 0.5 to 7.5 mm below the top surface. Hardness was highest 0.5 mm from the top surface at 342 HV. However, average hardness from 0.5 to 7.5 mm below the substrate surface was within $+5/-4$ HV of 337 HV. Near the bottom of the build, at 8.5 mm from the top

surface, average hardness increased to 352 HV before falling to the substrate hardness of 326 HV.

IV. DISCUSSION

A. Macrostructure

The macrostructure was characterized by columnar prior-beta grains and visible reheating bands. The formation of elongated prior- β grains extending from the bottom to the top surface of the build is commonplace in AM builds. Their formation is attributed to epitaxial growth on each successive layer, which was

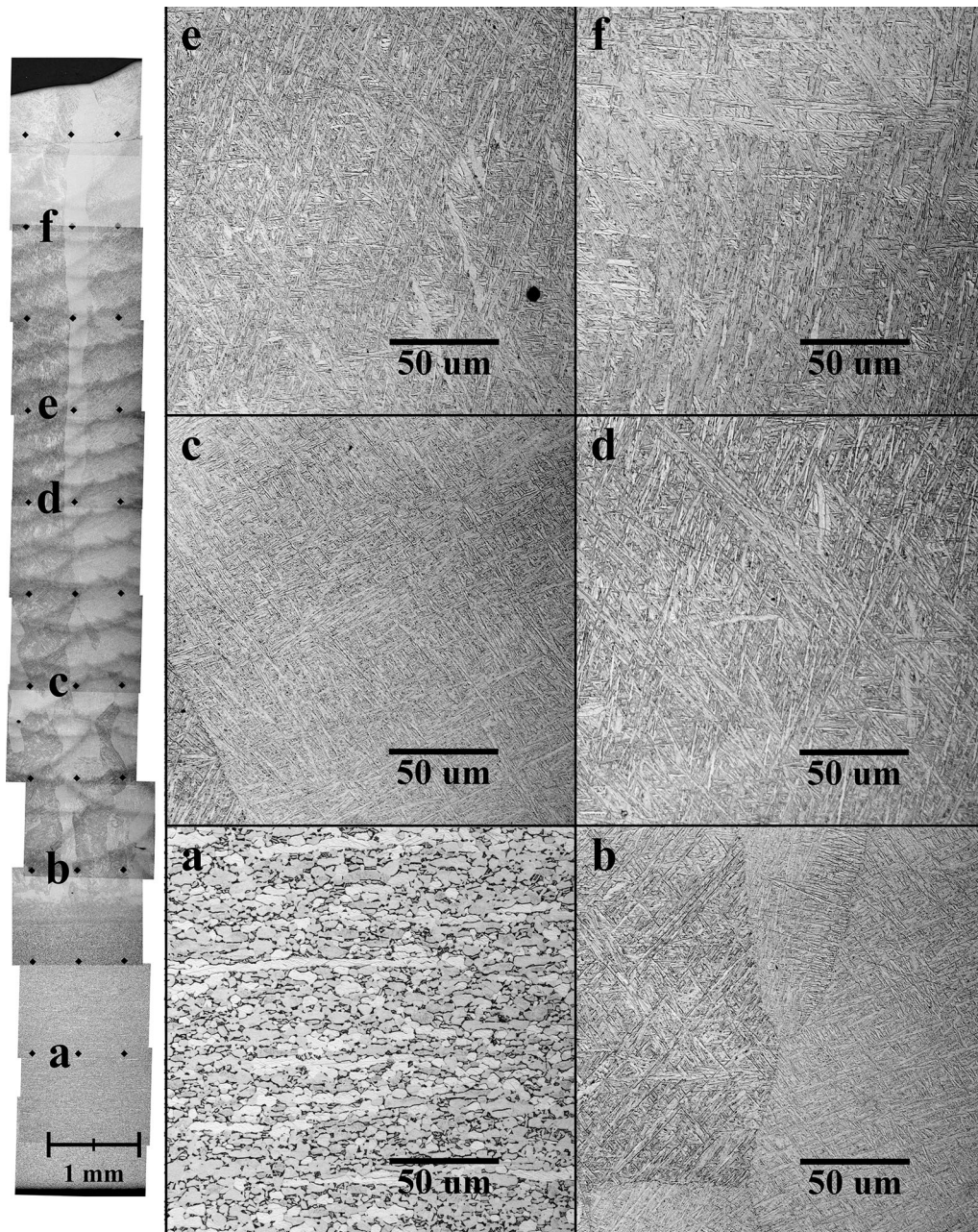


Fig. 5—Micrographs of the build processed using a pulsed laser beam. High-magnification images are shown for the locations indicated on the left-hand-side of the figure.

parallel to the heat gradient—see References 4, 19 for discussions regarding the formation and evolution of prior- β in additively manufactured Ti-6Al-4V. Laser-beam pulsing had no apparent effect on the epitaxial growth of the grains or their orientation.

Pulsing did, however, influence the shape of reheating bands (evident in Figures 4 and 5). In the case of the CW build, bands continued from hatch to hatch across the length of the build. In the pulsed-beam build, bands were semi-circular and overlapping from hatch to hatch. This reaffirms Kelly and Kemps findings^[8,9] that banding does not occur during the deposition of the layer on which it is observed, but rather result from reheating a

buried layers above the α dissolution temperature during the deposition of subsequent layers. Given this and the observation that bands were observed nearly to the top of the pulsed-beam build, we conclude that reheating of buried layers was reduced in the pulsed-beam deposited build.

One factor which contributed to reduce reheating of buried layers in the pulsed-beam build is total deposition time. Although the energy input per unit traverse length was identical for both builds, the total deposition time was doubled for the pulsed-beam build. Given the difference in total deposition time, and identical total energy input (assuming the laser absorption for both

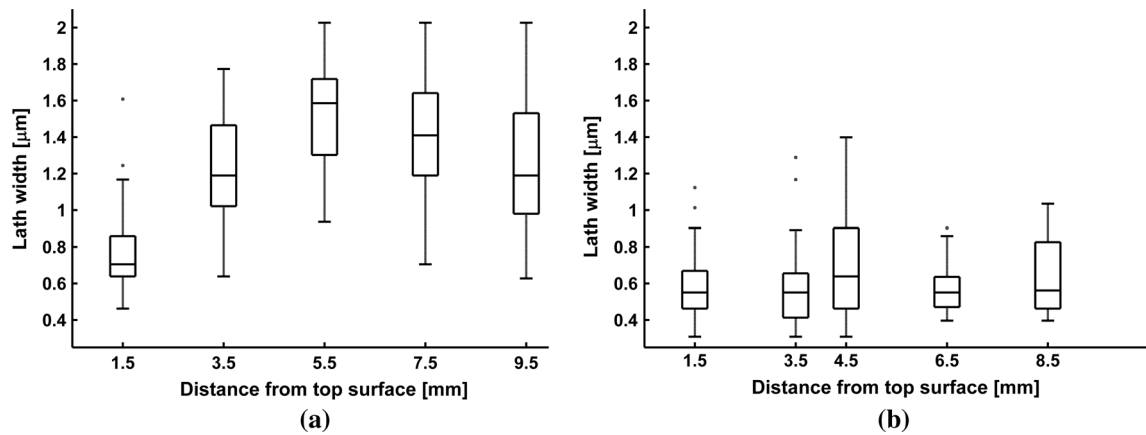


Fig. 6—Box plot of α -lath widths. The center, horizontal line within each box is the median, box edges represent the 25th and 75th percentiles, whiskers represent the range of data points considered. Individual points represent outliers.

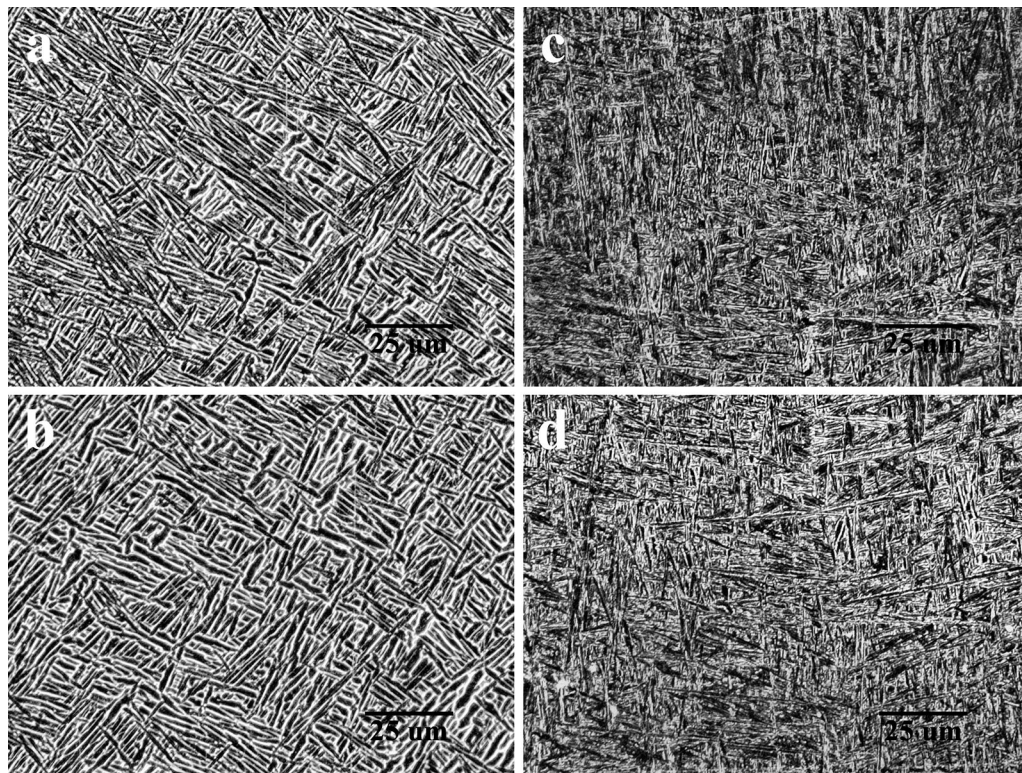


Fig. 7—Microstructure within a banded region (*a*, *c*) and in a region between reheating bands (*b*, *d*). Images to the left (*a*, *b*) show the microstructure for the CW AM build while those on the right (*c*, *d*) were taken from the pulsed AM build.

processes were equal), the pulsed-beam build was cooler. This may also be a factor in the reduced total build height of the pulsed-beam build (9.65 mm) compared with the CW build (9.93 mm) by affecting melt pool size and hence powder capture efficiency.

B. Microstructure

Beam pulsing strongly affected the width of α -laths. Within the CW build, α -laths were approximately 1.3 to 2.5 times wider than in the pulsed-beam build. In addition to being thinner, α -lath widths were also more uniform

throughout the pulsed-beam build. It is well known that the size and orientation of grains within a molten pool are controlled by solidification parameters: growth rate (R), thermal gradient (G), and undercooling (ΔT). In CW processes, the growth rate is defined by the weld-pool geometry and traversing speed. Since the solidification front cannot move faster than the traveling speed of the laser, the growth rate is always below the welding speed. The cooling rate (dT/dt) is the product of GR.

For CW processes, the cooling rate at the center line of a weld can be approximated using the Rosenthal solution (Eq. [1]).^[20] Using a speed, v , of 10.58 mm/s, a

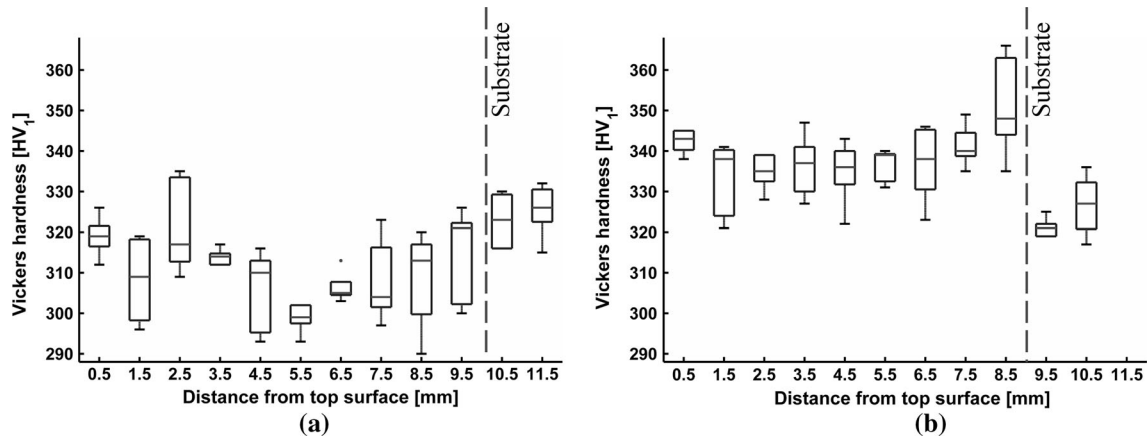


Fig. 8—Box plot of hardness data on (a) CW processed build and (b) pulsed-beam deposited build.

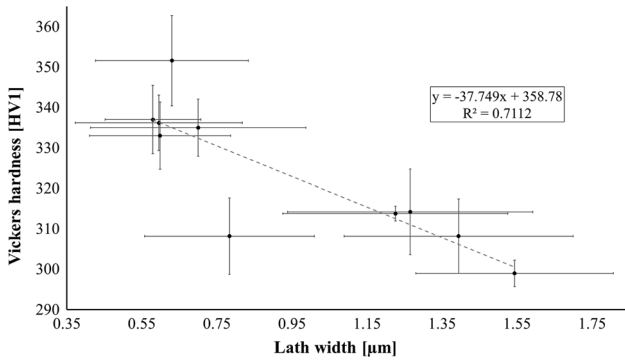


Fig. 9—All measured lath widths and Vickers hardness values. A linear model explains 71 pct of the variation in hardness with α -lath width.

thermal conductivity, k , of 6.7 W/mK, an absorption coefficient, α , of 0.4, a power, Q , of 450 W, a solidus temperature, T , of 1877 K (1604 °C), and room temperature, T_0 , of 293 K (20 °C), the cooling rate at the center line was approximately 6.2×10^3 K/s.

$$\frac{dT}{dt} = -2\pi k \frac{v}{\alpha Q} (T - T_0)^2. \quad [1]$$

During pulsed-beam processing, cooling rates are determined by multiple melting and solidification cycles. Cooling rates are expected to be higher than in CW processing, but their estimation requires numerical simulation.^[21] Higher cooling rates in the case of pulsed-beam processing may explain the finer microstructure within the pulsed-beam build. Another contributing factor may be stirring within the melt pool due to laser pulsing. If the solidification rate was such that the melt pool remained molten between laser pulses, laser pulsing would have induced melt flow due to fluctuating vapor pressure and melt temperatures. This stirring within the melt pool, as in the case of arc modulation,^[15] and magnetic stirring^[16] in arc-welding, likely contributed to the observed grain refinement within the pulsed-beam build, compared to the CW build.

According to Ahmed and Rack,^[22] cooling rates above 410 K/s should result in a $\beta \rightarrow \alpha'$ transformation in Ti-6Al-4V upon solidification. Given this, the microstructures in both the CW and pulsed-beam build should have been fully martensitic upon solidification. However, following solidification, the microstructure in both builds continued to be affected by heating and cooling cycles due to subsequent deposition paths. These thermal cycles resulted in aging and likely resulted in decomposition of martensitic α' , formed upon initial solidification. Multiple heating and cooling cycles in AM builds have also been shown by others to result in the growth of alpha grains and the formation of reheating bands.^[8,9] This mechanism, coupled with changing thermal conditions as the build progressed, was likely responsible for the non-uniformity in α -lath widths and microhardness observed in the CW build. Given that there was less variation in α -lath widths and microhardness in the pulsed-beam build, it is concluded that aging effects were reduced and microstructure was made more homogeneous throughout the build as a result of pulsed-beam processing.

C. Indentation Hardness

Measured indentation hardness followed similar trends to α -lath widths in both builds. This is not surprising given that mechanical properties of Ti-6Al-4V have been shown to be a function of α -lath width. For example, it has been shown that yield strength of AM build correlates linearly with (alpha-lath width)^{-0.5}.^[4] A reduction in alpha-lath width is thus expected to result in higher indentation hardness values. A plot of measured hardness values (for both builds) as a function of lath widths is given in Figure 9. A linear model explains 71 pct of the variation (correlation coefficient $R = -0.84$) in hardness with α -lath width.

V. CONCLUSIONS

The microstructure and indentation hardness of two directed-energy AM builds deposited on an Optomec

LENS system were compared. Each was processed with identical energy input per unit length but using a laser operating in CW or pulsed-beam mode. The CW build exhibited a statically significant variation in α -lath widths and indentation hardness with build height. In contrast to this, the pulsed-beam build produced finer α -laths, was harder, and had no statistically significant variation in α -lath widths or indentation hardness with build height.

The smaller and more uniform α -lath widths in the pulsed-beam build were due to rapid cooling within the melt pool, possibly a greater degree of melt pool stirring, and reduced thermal aging. Understanding the impact of each of these factors will require numerical simulation of melt pool dynamics and microstructural evolution during processing. This work suggests that pulsed-beam AM may be useful in forming builds with refined microstructures and uniform microstructure and mechanical properties.

ACKNOWLEDGMENTS

We acknowledge Edward A. Good for assistance in preparing metallographic samples. Funding for this work was provided by the Office of Naval Research, under Contract No. N00014-11-1-0668.

REFERENCES

1. Terry T Wohlers and Wohlers Associates: Wohlers Report 2014: Additive Manufacturing and 3D Printing State of the Industry: Annual Worldwide Progress Report, Wohlers Associates, Fort Collins, Colorado, 2014.
2. ASTM F42 Committee: Terminology for Additive Manufacturing Technologies, ASTM International, West Conshohocken, 2012.

3. G. Lütjering: *Mater. Sci. Eng. A*, 1998, vol. 243, pp. 32–45.
4. S.S. Al-Bermani, M.L. Blackmore, W. Zhang, and I. Todd: *Metall. Mater. Trans. A*, 2010, vol. 41A, pp. 3422–34.
5. L.E. Murr, E.V. Esquivel, S.A. Quinones, S.M. Gaytan, M.I. Lopez, E.Y. Martinez, F. Medina, D.H. Hernandez, E. Martinez, J.L. Martinez, S.W. Stafford, D.K. Brown, T. Hoppe, W. Meyers, U. Lindhe, and R.B. Wicker: *Mater. Charact.*, 2009, vol. 60, pp. 96–105.
6. N. Hrabec and T. Quinn: *Mater. Sci. Eng. A*, 2013, vol. 573, pp. 271–77.
7. L. Qian, J. Mei, J. Liang, and X. Wu: *Mater. Sci. Technol.*, 2005, vol. 21, pp. 597–605.
8. S.M. Kelly and S.L. Kampe: *Metall. Mater. Trans. A*, 2004, vol. 35A, pp. 1861–67.
9. S.M. Kelly and S.L. Kampe: *Metall. Mater. Trans. A*, 2004, vol. 35A, pp. 1869–79.
10. S. Lathabai, M. Glenn, C. MacRae, and D. Ritchie: *Aeromat 25 Conf. Expo. Am. Soc. Met.*, Orlando, FL, 2014.
11. M. Griffith, M.E. Schlienger, L.D. Harwell, M.S. Oliver, M.D. Baldwin, M.T. Ensz, and D.V. Nelson: *Solid Free. Fabr. Symp. Proc.*, Austin, TX, 1998.
12. J. Brooks, C. Robino, T. Headley, S. Good, and M. Griffith: *Proc. Solid Free. Fabr. Symp.*, Austin, TX, 1999, pp. 375–82.
13. R.S. Kircher, A.M. Christensen, and K.W. Wurth: *Solid Free. Fabr. Proc.*, Austin, TX, 2009, pp. 398–405.
14. F. Ghaini, M. Hamed, M. Torkamany, and J. Sabbaghzadeh: *Scripta Mater.*, 2007, vol. 56, pp. 955–58.
15. S. Sundaresan, G.D. Janaki Ram, and G. Madhusudhan Reddy: *Mater. Sci. Eng. A*, 1999, vol. 262, pp. 88–100.
16. M. Malinowski-Brodnicka, G. Den Ouden, and W.J.P. Vink: *Weld. J.*, 1990, vol. 69, pp. 52s–59s.
17. G. Madhusudhan Reddy, Amol.A. Gokhale, and K. Prasad Rao: *J. Mater. Sci.*, 1997, vol. 32, pp. 4117–26.
18. S. Mitzner, S. Liu, M. Domack, and R. Hafley: *Solid Free. Fabr. Proc.*, Austin, TX, 2012, pp. 536–55.
19. A.A. Antonysamy, J. Meyer, and P.B. Prangnell: *Mater. Charact.*, 2013, vol. 84, pp. 153–168.
20. Daniel. Rosenthal: *Trans. Am. Soc. Mech. Eng.*, 1946, vol. 48, pp. 849–65.
21. T. Zacharia, S.A. David, J.M. Vitek, and T. DebRoy: *Metall. Trans. A*, 1989, vol. 20A, pp. 957–67.
22. T. Ahmed and H.J. Rack: *Mater. Sci. Eng. A*, 1998, vol. 243, pp. 206–11.